Scale-reduction rule without drop in the sensitivity of a silicon-based guided-wave optical pressure sensor using a micromachined diaphragm

Masashi Ohkawa
Takashi Sato
Niigata University
Faculty of Engineering
8050 Ikarashi 2-no-cho, Nishi-ku
Nigata 950-2181, Japan
E-mail: ohkawa@eng.niigata-u.ac.jp

Abstract. In this study, an original scale-reduction rule without a drop in the sensitivity of a guided-wave optical pressure sensor was obtained using a micromachined diaphragm. The sensor has a rectangular diaphragm as a pressure-sensitive structure and a sensing waveguide across the diaphragm. Its sensitivity is theoretically known to be strongly dependent on the dimensions of the diaphragm. According to the theoretical results, the sensitivity can be kept constant even if the diaphragm dimensions are reduced as long as both the aspect ratio and the characteristic length of the diaphragm remain constant. Here, the characteristic length is introduced as the cube of either width or length of the rectangular diaphragm divided by the square of its thickness. Such a scale-reduction rule would be very useful for miniaturizing a sensor without reducing sensitivity, although it has not been experimentally confirmed. In this study, the scale-reduction rule was experimentally examined using three fabricated sensors with the same aspect ratio and the same characteristic length. The measured sensitivities of the three sensors were quite similar to each other, as theoretically predicted. [DOI: 10.1117/1.OE.51.1.014401]

Subject terms: integrated optics; pressure sensor; diaphragm; MOEMS; elasto-optic effect.

Paper 111147P received Sep. 16, 2011; revised manuscript received Nov. 22, 2011; accepted for publication Nov. 30, 2011; published online Feb. 7, 2012.

1 Introduction

Micro-opto-mechanical devices received considerable attention for the development of silicon micromachining technology.[1] A guided-wave optical pressure sensor with a micromachined diaphragm is one of the most promising micro-opto-mechanical devices. Several groups have reported on the integrated optic pressure sensors with diaphragms since the late 1980s.[2–5] Our group has been developing a silicon-based guided-wave optical pressure sensor with a diaphragm based on the elasto-optic effect.[6] One of the goals of our study is to develop a sensor that can be incorporated into a catheter for blood pressure measurements. Our demonstrated sensors are, however, sizable, although they have enough sensitivity to measure blood pressure. Therefore, in order to realize a catheter-tip blood pressure sensor, it is very important to miniaturize the sensor without sacrificing sensitivity. This motivates us to establish guidelines to reduce the diaphragm dimensions while keeping sensitivity constant.

Incidentally, the sensor sensitivity is known to be proportional to the cube of either the width or length of the rectangular diaphragm, both experimentally and theoretically.[7] Also, its sensitivity is inversely proportional to the square of the diaphragm thickness.[8] Based on these dependencies, an original scale-reduction rule without sensitivity loss can be derived; i.e., sensitivity can be maintained when the diaphragm dimensions are reduced by maintaining the aspect ratio: in other words, the width-to-length ratio and the characteristic length constant. Here, the characteristic length is defined as the cube of either the width or length of the diaphragm divided by the square of its thickness. To experimentally confirm the scale-reduction rule, three sensors were fabricated with diaphragms of the same aspect ratio and the same characteristic length. The exact diaphragm dimensions were 2.0 mm × 10.0 mm × 35 μm (sensor #1), 2.5 mm × 12.5 mm × 49 μm (sensor #2), and 3.0 mm× 15.0 mm × 64 μm (sensor #3). The sensitivities of sensors #1, #2, and #3 were 71, 72, and 69 mrad/kPa, respectively, at the waveguide position at the center of the diaphragm. Moreover, for other corresponding waveguide positions of the three sensors, the measured sensitivities were quite similar to each other as predicted by the scale-reduction rule.

2 Principles of Sensor Operation

Figure 1 shows a silicon-based guided-wave optical pressure sensor that consists of a micromechanical diaphragm and a straight single-mode waveguide across the diaphragm. The diaphragm is distorted when a pressure difference is applied to the diaphragm. This distortion causes strain, which induces a change in the refractive index of the diaphragm due to the elasto-optic effect. The index change yields phase retardation in the lightwave that propagates in the waveguide of the diaphragm. Since the phase retardation is generally dependent on the guided modes, that is, the fundamental TM-like and TE-like modes, the phase difference between the two modes is also a function of the applied pressure. To detect the phase difference, the sensor is placed between a pair of crossed polarizers, as shown in Fig. 1. The polarization axis of the input polarizer is oriented at

0091-3286/2012/$25.00

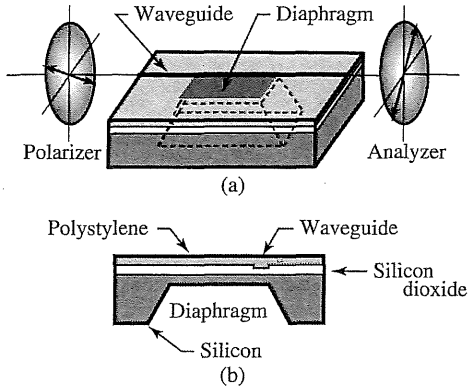

Fig. 1 (a) Schematic drawing of a silicon-based guided-wave optical pressure sensor placed between a pair of crossed polarizers and (b) its cross-sectional view.

45 deg with respect to the polarization of each guided mode, so that the laser beam is coupled to the TM-like and TE-like modes at equal intensities. The lightwave has linear, elliptical, or circular polarization at the end of the waveguide, corresponding to the induced phase difference between the two guided modes. The intensity of the light beam passing through the output polarizer sinusoidally changes with the applied pressure. Therefore, the applied pressure can be determined from the output intensity.

3 Theoretical Results

3.1 *Sensitivity Dependence to the Diaphragm Dimensions*

3.1.1 *Sensitivity versus side length of the diaphragm*

The phase sensitivity, that is, the induced phase difference per unit pressure, is strongly dependent on the diaphragm width and length. The phase sensitivity was calculated, using the mathematical description provided in Appendix, as a function of the width of the rectangular diaphragm while keeping the aspect ratio and the thickness of the diaphragm constant. In this calculation, a rectangular diaphragm with width, a, length b, and thickness, t, was assumed, as shown in Fig. 2. It was also assumed that the waveguide was placed parallel to the diaphragm edge, b, and that the pressure was uniformly applied over the diaphragm with all edges rigidly clamped. The wavelength of the guided light was set at 633 nm. Incidentally, theoretical calculations should be carried out using the mechanical and optical parameters of the materials of which the sensor is comprised. However, the parameters for polystyrene, which was the material used for the guided layer of the waveguide shown in Fig. 1, have yet to be determined. In this study, the parameters of fused silica were used instead of those of polystyrene.[9] The numerical result obtained by using the parameters of fused silica should hold qualitatively true for a sensor with a polystyrene waveguide.

Figure 3 indicates the calculated phase sensitivity as a function of the diaphragm width, a, for waveguide position at the diaphragm edge where the sensitivity is the highest. Sensitivity is normalized to be at unity at a width of 1 mm. From Fig. 3, the slope is 3 in the log-log graph because sensitivity is proportional to the cube of the diaphragm width a. Such a relationship between the normalized phase sensitivity and the width, a, is valid for the arbitrary aspect ratio, a/b,

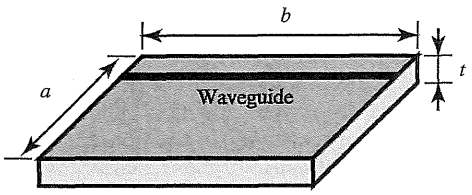

Fig. 2 Illustration of a rectangular diaphragm assumed in the calculations.

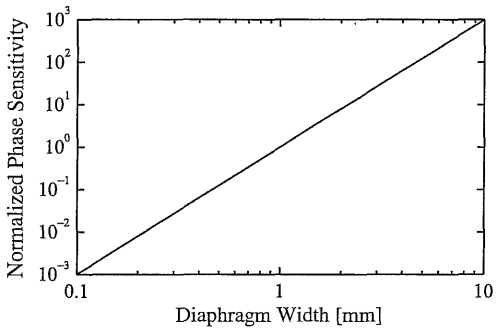

Fig. 3 Calculated phase sensitivity as a function of the width of diaphragm. The phase sensitivity is normalized to be at unity at 1 mm in width.

and thickness, t, of the diaphragm, according to further theoretical considerations. This relationship can be also applied to any waveguide position, although the sensitivity is dependent on the waveguide position.

3.1.2 *Sensitivity versus diaphragm thickness*

The phase sensitivity was calculated as a function of the diaphragm thickness, t, with the other dimensions remaining constant. Figure 4 shows the calculated phase sensitivity for a waveguide located at the diaphragm edge. The phase sensitivity is normalized to be at unity at a thickness of 10 μm. In Fig. 4, the slope is -2 in the log-log graph because the sensitivity is inversely proportional to the square of the diaphragm thickness, if the diaphragm thickness is considerably greater than the waveguide thickness, which was assumed to be 1 μm in the calculation. When the diaphragm thickness is comparable to or less than the extent of the guided light in the direction of the thickness, the sensitivity

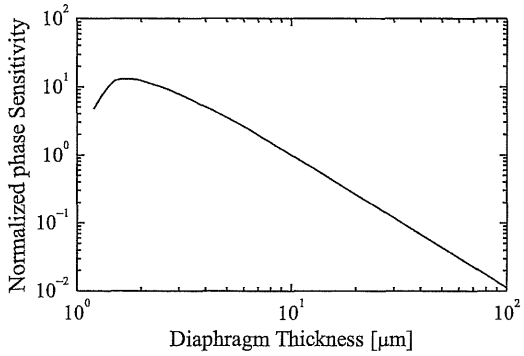

Fig. 4 Calculated normalized phase sensitivity as a function of the thickness of diaphragm. The phase sensitivity is normalized to be at unity at 10 μm in thickness.

decreases as the diaphragm thins because the overlap integral between the electric field of the guided light and the refractive index change becomes smaller.[7] When a considerably thin diaphragm is employed, attention should be paid to the excess decrease of sensitivity. In addition, such a relationship between the normalized phase sensitivity and the diaphragm thickness, t, is valid for any aspect ratio and waveguide position.

3.2 *Scale-Reduction Rule of the Diaphragm Without Sensitivity Loss*

To design a miniaturized sensor, a scale-reduction rule for the diaphragm dimensions without sacrificing sensitivity is very helpful, especially when the sensor is sufficiently sensitive but sizable. From Sec. 3.1.1, we were able to show that sensitivity is proportional to the cube of the diaphragm width, a, if the aspect ratio, a/b, and the thickness, t, remain constant. Also, from Sec. 3.1.2, sensitivity is inversely proportional to the square of the diaphragm thickness, t, when the aspect ratio, a/b, and the width, a, are both kept constant. Here, the characteristic length, a^3/t^2, is introduced, as defined by the cube of the diaphragm width, a, divided by the square of the thickness, t. According to the two theoretical results, sensitivity can remain constant, even if the diaphragm dimensions are reduced, as long as both the aspect ratio and the characteristic length remain constant.

4 Experiments

4.1 *Fabrication and Measurements*

We fabricated three sensors with diaphragms of 2.0 mm × 10.0 mm × 35 μm (sensor #1), 2.5 mm × 12.5 mm × 49 μm (sensor #2), and 3.0 mm × 15.0 mm × 64 μm (sensor #3) to confirm the scale-reduction rule mentioned above. The aspect ratio, a/b, and the characteristic length, a^3/t^2, of the three sensors were 0.2 and approximately 6.5 m, respectively. The waveguides were spaced 0.1 mm apart from each other in order to concurrently determine sensitivity dependences on waveguide position. In this fabrication, a silicon substrate was thermally oxidized at 1100 °C to form a 1.0 μm-thick silicon dioxide layer. The silicon dioxide layer was selectively removed with an etchant of buffered hydrofluoric acid using a patterned photoresist as an etching mask. Then, the exposed silicon was anisotropically etched in aqueous potassium hydroxide solution at 50 °C to produce the diaphragm. After diaphragm formation, the 1.0-μm-thick silicon dioxide layer was regrown by thermal oxidation to serve as the buffer layer in order to sufficiently negate radiation loss of the guided waves in the silicon substrate. Shallow 10-μm-wide and 0.1-mm-deep grooves were engraved on the silicon dioxide layer, parallel to the diaphragm edge, using buffered hydrofluoric acid. The polystyrene layer was spin-coated as the guided layer, and its thickness at the grooves was 1.1 μm.

Figure 5 illustrates the experimental setup used to measure output power versus applied pressure. The fabricated sensors were tested using a linearly polarized He-Ne laser at 633 nm. The polarization of the laser beam was set at 45 deg to the sensor surface, so that the input polarizer, shown in Fig. 1, was not utilized in this experiment. The output light from the sensor was detected by a photodetector, after being passed through a pinhole to block stray light. In order to apply pressure to the diaphragm, a syringe was connected to the sensor by a silicone tube. The pressure difference, ranging from −40 to 40 kPa, was exerted on the diaphragm by pulling and pushing on the plunger, and was determined from the ideal gas law. A positive value indicates that the pressure in the etched hole is higher than that in the atmosphere.

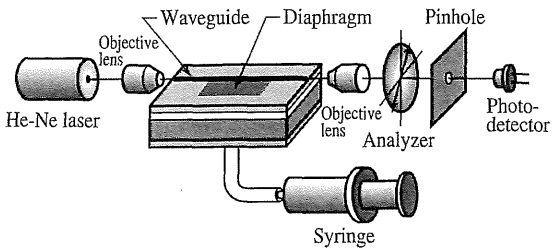

Fig. 5 Experimental setup used to measure the output intensity with respect to the applied pressure.

4.2 *Experimental Results*

4.2.1 *Sensor #1*

Figure 6 shows the experimental results for sensor #1 with a 2.0 mm × 10.0 mm × 35 μm diaphragm. Figures 6(a) and 6(b) are for the waveguides nearest to the diaphragm edge and nearest to the center of the diaphragm, respectively. The solid line in each figure shows the computerized projection of the experimental data. The halfwave pressure was evaluated as the half-period of the output intensity, which corresponds to a phase difference of π rad. From the halfwave pressure, the phase sensitivity, as defined as the resultant phase difference per unit pressure, was calculated. From

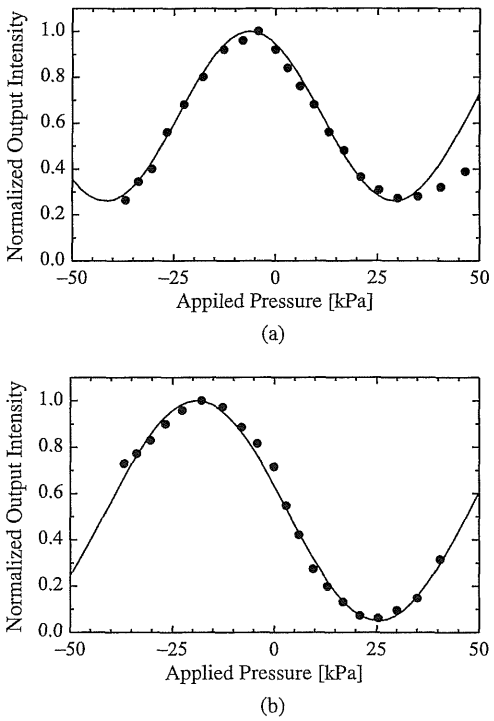

Fig. 6 Measured output intensity versus applied pressure for waveguides located (a) nearest to the diaphragm edge and (b) nearest to the center of the diaphragm in sensor #1.

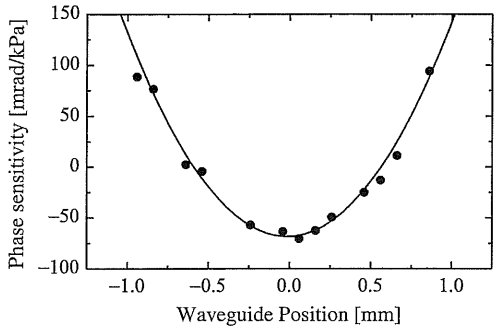

Fig. 7 Measured sensitivity as a function of waveguide position in sensor #1. Waveguide positions of ±1 mm approximately correspond to the edge of the diaphragm, while a waveguide position of 0 mm corresponds to the center.

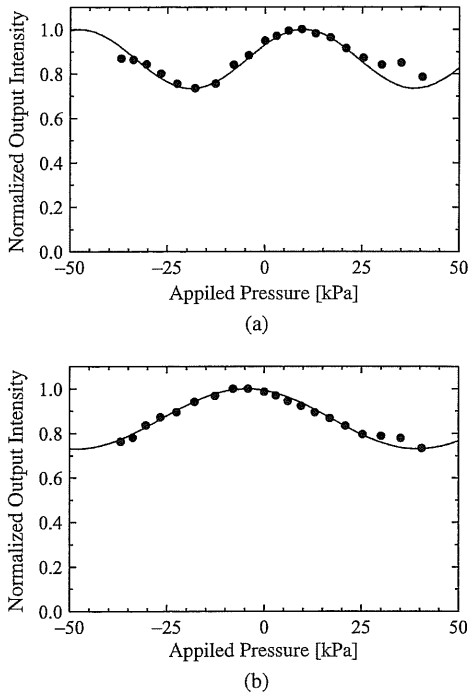

Fig. 8 Measured output intensity versus applied pressure for waveguides located (a) nearest to the diaphragm edge and (b) nearest to the center of the diaphragm in sensor #2.

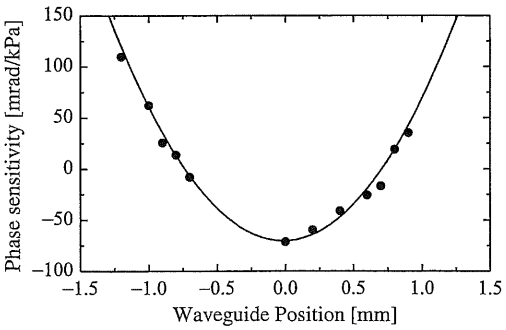

Fig. 9 Measured sensitivity as a function of waveguide position in sensor #2. Waveguide positions of ±1.25 mm approximately correspond to the edge of the diaphragm, while a waveguide position of 0 mm corresponds to the center.

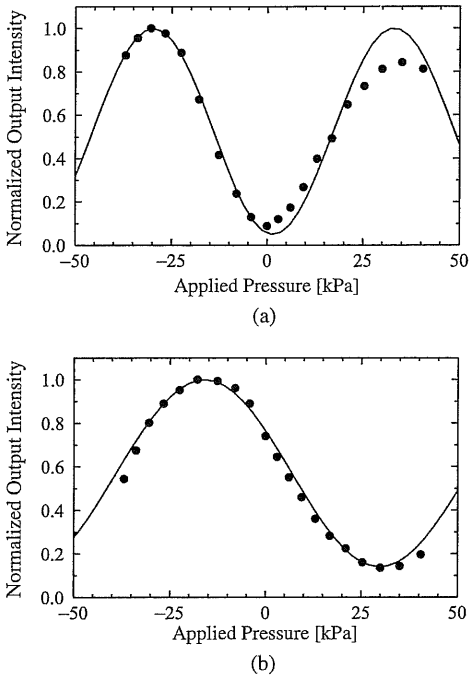

Fig. 10 Measured output intensity versus applied pressure for waveguides located (a) nearest to the diaphragm edge and (b) nearest to the center of the diaphragm in sensor #3.

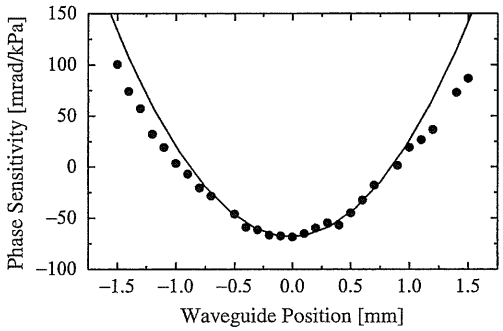

Fig. 11 Measured sensitivity as a function of waveguide position in sensor #3. Waveguide positions of ±1.5 mm approximately correspond to the edge of the diaphragm, while a waveguide position of 0 mm corresponds to the center.

Figs. 6(a) and 6(b), the halfwave pressures are 36 and 44 kPa, and the corresponding phase sensitivities were calculated as 89 and 71 mrad/kPa, respectively. Moreover, the phase sensitivities of the other waveguide positions were also measured. Figure 7 indicates the measured phase sensitivities as a function of the waveguide position. Several data points are missing due to imperfect waveguides. In Fig. 7, the theoretical curve reflects the calculated results when the aspect ratio of diaphragm is 0.2. The sign of the measured phase sensitivity was determined based on the theoretical sensitivity, although it cannot be distinguished in these experimental results.

4.2.2 *Sensor #2*

Figures 8(a) and 8(b) show the experimental results of sensor #2 with a 2.5 mm × 12.5 mm × 49 μm diaphragm for the

Table 1 Sensitivities of the three sensors with different diaphragm dimensions for the waveguides nearest to the edge and center.

		Sensor #1	Sensor #2	Sensor #3
Diaphragm dimensions	Width a (mm)	2.0	2.5	3.0
	Length b (mm)	10	12.5	15
	Thickness t (μm)	35	49	64
Width-length ratio a/b			0.2	
Characteristic length a^3/t^2 (m)		6.5	6.4	6.6
Sensitivity for waveguide nearest to edge (mrad/kPa)		89	110	100
Sensitivity for waveguide nearest to center (mrad/kPa)		−71	−72	−69

waveguides located nearest to the edge and nearest to the center of the diaphragm, respectively. From Figs. 8(a) and 8(b), the halfwave pressures are 29 and 44 kPa, corresponding to the sensitivities of 110 and 72 mrad/kPa, respectively. Figure 9 shows the measured sensitivity versus the waveguide position. Several data points are missing due to imperfect waveguides, similar to the results of sensor #1. The solid curve in the figure indicates the computerized projection where $a/b = 0.2$.

4.2.3 *Sensor #3*

Figure 10 shows the experimental results of sensor #3 with a 3.0 mm × 15.0 mm × 64 μm diaphragm. The waveguides of Figs. 10(a) and 10(b) were located nearest to the diaphragm edge and nearest to the center, respectively. The halfwave pressure was evaluated as 31 and 46 kPa, as shown in Figs. 10(a) and 10(b), corresponding to sensitivities of 100 and 69 mrad/kPa respectively. Figure 11 shows the measured phase sensitivity versus the waveguide position, and the theoretical curve reflecting the calculated results when $a/b = 0.2$.

4.3 *Discussion*

In Figs. 7, 9, and 11, the relationships between the measured phase sensitivity and the waveguide position are almost identical to the theoretical predictions, although there is a slight difference near the diaphragm edge in Fig. 11. In sensor #3, it is speculated that the waveguides were slightly oblique with respect to the diaphragm edge. For each sensor, the largest sensitivity was obtained for the waveguide nearest the diaphragm edge, as theoretically predicted.[9] The sensitivity, however, rapidly decreased as the waveguide deviated from the edge. In contrast, near the center of the diaphragm, small deviations in the waveguide had a minimal affect on the sensitivity. By comparing the sensitivities of the fabricated sensors, the center of the diaphragm is better than the edge because this placement avoid the effects of waveguide misalignment.

Table 1 shows the sensitivities of the fabricated sensors for the waveguides nearest to the edge and nearest to the center. Nearest to the center of the diaphragm, the measured sensitivities are quite similar to each other, as predicted by the scale-reduction rule. Regarding the sensitivities nearest to the diaphragm edge, there is a difference of about 20 mrad/kPa. This difference was mainly caused by deviations in the waveguide from the edge, as well as slanted waveguides with respect to the diaphragm edge. Even for the measured sensitivities nearest to the edge, it is presumed that the sensitivities would be similar to each other, less error due to waveguide deviation. Therefore, the proposed scale-reduction rule is verified by the experimental results of the three fabricated sensors.

Incidentally, the obtained sensitivities of the three sensors are sufficient for blood pressure measurement, in which a phase sensitivity of about 80 mrad/kPa, which corresponds to approximately 1 rad per 100 mmHg, would be necessary. But, the sensors must be further miniaturized in order to be incorporated into a catheter. According to the scale-reduction rule, a sensor with a 0.5 mm × 2.5 mm × 4.4 μm diaphragm is expected to have the same sensitivity as the fabricated sensors and could be put into a catheter. However, for such a thin multi-layered diaphragm consisting of silicon and thermal silicon dioxide layers, the scale-reduction rule may not be applied due to built-in thermal stress and sensitivity degradation, as described in Sec. 3.1.2. Consequently, further detailed consideration is required to design a miniaturized sensor that could be incorporated into a catheter.

5 Conclusions

We experimentally examined a scale-reduction rule without sensitivity loss in a silicon-based guided-wave optical pressure sensor. It was found, both theoretically and experimentally, that sensitivity does not change even if the diaphragm dimensions are reduced as long as the aspect ratio and characteristic length remain constant. Miniaturization under the scale-reduction rule has an additional advantage of broadening the dynamic range of which the upper limit is restricted by the resonance frequency of diaphragm. Since the resonance frequency is inversely proportional to the square of either the width or length of the rectangular diaphragm and is proportional to the diaphragm thickness, the resonance frequency gets higher without sensitivity decrease if the diaphragm is miniaturized under the scale-reduction rule.

Appendix: Theoretical Formulas

In this appendix, the numerical formulas used to calculate sensitivity versus diaphragm dimensions are briefly described.[9] It is assumed that the diaphragm has a square shape with a side length of a and a thickness of h, and all edges of the diaphragm are rigidly clamped. Regarding the coordinate axis, the y-z plane lies in the middle plane between the two surfaces of the diaphragm, and the z-axis is parallel to the waveguide. The x-axis is perpendicular to the plate surface.

Deflection, w, of the diaphragm, in other words, displacement from equilibrium, due to uniformly applied pressure, q, is obtained from the differential equation:

$$\frac{\partial^4 w}{\partial y^4} + 2\frac{\partial^4 w}{\partial y^2 \partial z^2} + \frac{\partial^4 w}{\partial z^4} = \frac{q}{D}, \tag{1}$$

where D is flexural rigidity, defined as $D = Eh^3/12(1-\mu^2)$.[10] Also, E and μ are the modulus of elasticity and the Poisson's ratio, respectively. From the obtained deflection, the distribution of stress in the diaphragm is derived. Next, the strain distribution, S, is calculated from the stress distribution, assuming that Hooke's law is applicable. The anisotropic index change, Δn_i, caused by the induced strain is given by

$$\Delta n_i = -\frac{1}{2} n^3 p_{ij} S_j \qquad (i,j = 1, \cdots, 6), \tag{2}$$

where p_{ij} denotes each component of the elasto-optic tensor. The strain has six components, which are divided into two kinds of strain: normal strain in the x, y, and z directions with subscripts 1, 2, and 3, respectively, and shearing strain with subscripts 4 through 6. Difference in phase retardations in the two guided waves, such as TM-like and TE-like modes, is given by Δn_1 and Δn_2. The amount of phase difference, $\Delta\phi$ between them is expressed as

$$\Delta\phi = \Delta\phi_{\mathrm{TM}} - \Delta\phi_{\mathrm{TE}}, \tag{3}$$

where

$$\Delta\phi_{\mathrm{TM}} \approx \int_{-b/2}^{b/2} \left(\frac{\omega\varepsilon_0}{4} \int_{-a/2}^{a/2} \int_{-t/2}^{t/2} E_x(x,y) \Delta n_1(x,y,z) \times E_x^*(x,y)\mathrm{d}x\mathrm{d}y \right) \mathrm{d}z, \tag{4}$$

$$\Delta\phi_{\mathrm{TE}} = \int_{-b/2}^{b/2} \left(\frac{\omega\varepsilon_0}{4} \int_{-a/2}^{a/2} \int_{-t/2}^{t/2} E_y(x,y) \Delta n_2(x,y,z) \times E_y^*(x,y)\mathrm{d}x\mathrm{d}y \right) \mathrm{d}z, \tag{5}$$

where ω is the angular frequency of the light, ε_0 is the permittivity of the vacuum, and * indicates the complex conjugate. Also, E_x and E_y are the power-normalized x-directed electric field component of the TM-like mode and the y-directed electric field component of the TE-like mode, respectively.

Acknowledgments

We would like to express our gratitude to Mr. Yuki Shirai, Mr. Takeshi Goto, and Mr. Atsushi Yamada for their detailed work in sensor fabrication and measurements. This work is, in part, supported by a grant-in-aid for scientific research (No. 22560322) from the Japan Society for the Promotion of Science.

References

1. M. Tabib-Azar and G. Beheim, "Modern trends in microstructures and integrated optics for communication, sensing, and actuation," *Opt. Eng.* **36**(5), 1307–1318 (1997).
2. M. Ohkawa, M. Izutsu, and T. Sueta, "Integrated optic pressure sensor on silicon substrate," *Appl. Opt.* **28**(23), 5153–5157 (1989).
3. G. N. De Brabander, J. T. Boyd, and G. Beheim, "Integrated optical ring resonator with micromechanical diaphragm for pressure sensing," *IEEE Photon. Technol. Lett.* **6**(5), 671–673 (1994).
4. G. N. De Brabander, G. Beheim, and J. T. Boyd, "Integrated optical micromachined pressure sensor with spectrally encoded output and temperature compensation," *Appl. Opt.* **37**(15), 3264–3267 (1998).
5. H. Porte et al., "Imbalanced Mach-Zehnder interferometer integrated in micromachined silicon substrate for pressure sensor," *J. Lightwave Technol.* **17**(2), 229–233 (1999).
6. M. Ohkawa et al., "Silicon-based integrated optic pressure sensor using intermodal interference between TM-like and TE-like modes," *Fiber and Integr. Opt.* **21**(2), 105–113 (2002).
7. H. Nikkuni et al., "Sensitivity dependences on side length and aspect ratio of a diaphragm in a glass-based guided-wave optical pressure sensor," *Opt. Express* **16**(19), 15024–15032 (2008).
8. H. Nikkuni et al., "Sensitivity dependence with respect to diaphragm thickness in guided-wave optical pressure sensor based on elasto-optic effect," *Opt. Eng.* **47**(4), 044402 (2008).
9. M. Ohkawa et al., "Relationship between sensitivity and waveguide position on the diaphragm in integrated optic pressure sensors based on the elasto-optic effect," *Appl. Opt.* **41**(24), 5016–5021 (2002).
10. S. P. Timoshenko and S. Woinowsky-Krieger, *Theory of Plates and Shells*, McGraw-Hill Kogakusha, Tokyo (1981).

Masashi Ohkawa received his BE, ME, and DrEng degrees in electrical engineering from Osaka University, Japan, in 1984, 1986, and 1989, respectively. In 1989, he joined the Faculty of Engineering, Niigata University, Japan, as a research associate, and is currently a professor. His research interests include integrated optic devices and holography.

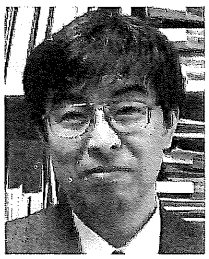

Takashi Sato received his BS, MS, and PhD in electronic engineering from Kyoto University in 1976, 1978, and 1983, respectively. He is currently a professor at Niigata University. His research areas are laser production of alkali hydride particles, frequency stabilization of dye lasers and semiconductor lasers, oscillation frequency shift in semiconductor lasers in magnetic fields, and the application of nonlinear optical effects for frequency stabilization of a semiconductor lasers.